Let them have CAKES: A Cutting-Edge Algorithm for Scalable, Efficient, and Exact Search on Big Data[*]

Morgan E. Prior[†], Thomas J. Howard III[‡], Oliver McLaughlin[‡], Terrence Ferguson[‡], Najib Ishaq[‡], and Noah M. Daniels[‡]

Abstract. The Big Data explosion has created a demand for efficient and scalable algorithms for similarity search. While much recent work has focused on *approximate* k-NN search, *exact* k-NN search has not kept up. We present CAKES, a set of three novel algorithms for exact k-NN search. CAKES's algorithms are generic over *any* distance function, and do not scale with the cardinality or embedding dimension of the dataset. Instead, they scale with geometric properties of the dataset–namely, metric entropy and fractal dimension– thus providing immense speed improvements over existing exact k-NN search algorithms when the dataset conforms to the manifold hypothesis. We demonstrate these claims by contrasting performance on a randomly-generated dataset against that on some datasets from the ANN-Benchmarks suite under commonly-used distance functions, a genomic dataset under Levenshtein distance, and a radio-frequency dataset under Dynamic Time Warping distance. CAKES exhibits near-constant running time on data conforming to the manifold hypothesis as cardinality grows, and has perfect recall on data in metric spaces. CAKES also has significantly higher recall than state-of-the-art k-NN search algorithms even when the distance function is not a metric. We conclude that CAKES is a highly efficient and scalable algorithm for exact k-NN search on Big Data. We provide a Rust implementation of CAKES.

MSC codes. 68P05, 68P10

1. Introduction.

Researchers are collecting data at an unprecedented scale. In many fields, datasets grow exponentially, and this increase in the rate of data collection outpaces improvements in computing performance as predicted by Moore's Law [20]. This indicates that the performance of computing systems will not keep pace with the growth of data. Often dubbed "the Big Data explosion," this phenomenon has created a need for better algorithms to analyze large datasets.

Examples of large datasets include genomic databases, time-series data such as radio frequency signals, and neural network embeddings. Large language models such as GPT [7, 27] and LLAMA-2 [33], and image embedding models [30, 10] are a common source of neural network embeddings. Among biological datasets, SILVA 18S [29] contains ribosomal DNA sequences of approximately 2.25 million genomes with an aligned length of 50,000 letters. Among time-series datasets, the RadioML dataset [28] contains approximately 2.55 million samples of synthetically-generated signals of different modulation modes.

Many researchers are interested in similarity search on these datasets. Similarity search enables a variety of applications, including recommendation [5] and classification systems [32]. As the cardinalities and dimensionalities of datasets have grown, however, efficient and accurate similarity search has become challenging; even state-of-the-art algorithms exhibit a steep

[*]Submitted to the editors DATE.

[†] Department of Mathematics, University of Rhode Island, Kingston, RI (meprior424@gmail.com)

[‡] Department of Computer Science and Statistics, University of Rhode Island, Kingston, RI (thoward27@uri.edu, olwmc@gmail.com, fergusontr@gmail.com, najib_ishaq@zoho.com, noah_daniels@uri.edu)

tradeoff between recall and throughput [24, 19, 5, 3].

Given some measure of similarity between data points, there are two common definitions of similarity search: k-nearest neighbor search (k-NN) and ρ-nearest neighbor search (ρ-NN). k-NN search aims to find the k most similar points to a query, while ρ-NN search aims to find all points within a similarity threshold ρ of a query. Previous works have used the term *approximate* search to refer to ρ-NN search, but in this paper, we reserve the term *approximate* for algorithms which do not exhibit perfect recall. In contrast, an *exact* search algorithm exhibits perfect recall.

k-NN search is one of the most ubiquitous classification and recommendation methods in use [12, 9]. Naïve implementations of k-NN search, whose time complexity is linear in the dataset's cardinality, prove prohibitively slow for large datasets. While fast algorithms for k-NN search on large datasets exist, they are often approximate [13], and while approximate search may be sufficient for some applications, the need for efficient and *exact* search remains [34]. For example, for a majority voting classifier, approximate k-NN search may agree with exact k-NN search for large values of k, but may be sensitive to local perturbations for smaller values of k. This is especially true when classes are not well-separated [38]. Further, there is evidence that distance functions which do not obey the triangle inequality, such as cosine distance, perform poorly for k-NN search in biomedical settings [16]; this suggests that approximate k-NN search could perform poorly in such contexts.

ρ-NN search also has a variety of applications. For example, one could search for all genomes within a maximum edit distance of a query genome to find evolutionarily-related organisms [8]. One could also search for all words within a maximum edit distance of a misspelled word to suggest corrections [35]. Given an advertisement and a database of user profiles, one could search for all users whose profiles are "similar enough" to target the advertisement [39]. GPS and other location-based services use ρ-NN search to find nearby points of interest [39] to a user's location.

This paper introduces CAKES (CLAM-Accelerated K-NN Entropy Scaling Search), a set of three novel algorithms for exact k-NN search. We also present improvements to the clustering and ρ-NN search algorithms in CHESS [18], as well as improved genericity across distance functions. We provide a comparison to several current algorithms for similarity search; namely, FAISS [19], HNSW [25], and ANNOY [5], on datasets from the ANN-benchmarks suite [3]. We further benchmark CAKES on a large genomic dataset, the SILVA 18S dataset [29], using Levenshtein [23] distance on unaligned genomic sequences, and a radio frequency dataset, RadioML [28], using Dynamic Time Warping (DTW) [14] distance on complex-valued time-series. Finally, we compare real-world datasets to an artificially-generated dataset obeying simple statistical properties.

1.1. Related Works. Recent k-nearest neighbor search algorithms designed to scale with the exponential growth of data include Hierarchical Navigable Small World networks (HNSW) [24], InVerted File indexing (FAISS-IVF) [1], random projection and tree building (ANNOY) [5], and entropy-scaling search [37, 18]. However, some of these algorithms do not provide exact search (as defined in Section 1 above).

Hierarchical Navigable Small World networks [24] relies on navigable small world (NSW) networks [22, 6] and skip lists. HNSW builds a multi-layered graph of the dataset. A query point and each data point are inserted into the graph and joined by an edge to the M nearest nodes in the in the graph, where M is a tunable parameter. The highest layer in which an element can be placed is determined randomly with an exponentially-decaying probability distribution. Search starts at the highest layer and descends to the lowest layer, greedily following a path of edges to the nearest node, until reaching the query point. To improve accuracy, the $efSearch$ hyperparameter can be changed to specify the number of closest nearest neighbors to the query vector to be found at each layer.

InVerted File indexing (IVF) [1, 31, 21] clusters data into high-dimensional Voronoi cells, and whichever cell a query point falls into is then searched exhaustively, similarly to an early precursor to our work [37]. The number of cells used is governed by the n_{list} parameter. Increasing this parameter decreases the number of points being exhaustively searched, so it improves speed at the cost of accuracy. To mitigate accuracy issues caused by a query point falling near a cell boundary, the algorithm has a tunable parameter n_{probe}, which specifies the number of additional adjacent or nearby cells to search.

ANNOY [5] relies on random projection and tree building for approximate k-NN search. At each intermediate node of the tree, two points are randomly sampled from the space, and the hyperplane equidistant from them is chosen to divide the space into two subspaces. This process iterates to create a forest of trees, and the number of iterations is a tunable parameter. At search time, one can increase the number of trees to be searched to improve recall at the cost of speed.

The entropy-scaling search paradigm exploits the geometric and topological structure inherent in large datasets. Importantly, as suggested by their name, entropy-scaling search algorithms exhibit asymptotic complexity that scales with topological properties of the dataset, instead of its cardinality. In 2019, we introduced CHESS (Clustered Hierarchical Entropy-Scaling Search) [18], which extended entropy-scaling ρ-NN search from a flat clustering approach to a hierarchical clustering approach. CLAM (Clustering, Learning and Approximation with Manifolds), originally developed to allow "manifold mapping" for anomaly detection [17], is a refinement of the clustering algorithm from CHESS. In this paper, we introduce CAKES, a set of three entropy-scaling algorithms for k-NN search, implemented in the Rust programming language.

2. Methods.

In this manuscript, we are primarily concerned with k-NN search in a finite-dimensional space. Given a dataset $\mathbf{X} = \{x_1 \dots x_n\}$ of cardinality $|\mathbf{X}| = n$, we define a *point* or *datum* $x_i \in \mathbf{X}$ as a singular observation. Examples include the neural-network embedding of an image, the genome of an organism, and a measurement of a radio frequency signal.

We define a *distance function* $f : \mathbf{X} \times \mathbf{X} \mapsto \mathbb{R}^+ \cup \{0\}$ which, given two points, deterministically returns a finite and non-negative real number. A distance of zero defines identity among points (i.e. $f(x, y) = 0 \Leftrightarrow x = y$) and larger values indicate greater dissimilarity among points. We also require that the distance function be symmetric (i.e., $f(x, y) = f(y, x)\ \forall\ x, y \in \mathbf{X}$). In addition to these constraints, if the distance function obeys the triangle inequality (i.e. $f(x, y) \leq f(x, z) + f(z, y)\ \forall\ x, y, z \in \mathbf{X}$), then it is also a *distance metric*. Similar to [37], when used with distance metrics, all search algorithms in CAKES are exact. For example, Euclidean, Levenshtein [23] and Dynamic Time Warping (DTW) [26] distances are all distance metrics, while cosine distance is not a metric because it violates the triangle inequality (e.g., consider the points $x = (1, 0)$, $y = (0, 1)$ and $z = (1, 1)$ on the Cartesian plane).

The choice of an appropriate distance function varies by dataset and domain. For example, with neural-network embeddings, one could use Euclidean (L2) or cosine distance. With genomic or proteomic sequence data, Levenshtein, Smith-Waterman, Needleman-Wunsch or Hamming distances are useful. With time-series data, one could use Dynamic Time Warping (DTW) or Wasserstein distance.

CAKES derives its advantages from the manifold hypothesis [11], the notion that high-dimensional data collected from constrained generating phenomena typically only occupy a low-dimensional manifold within their embedding space. We say that such data are *manifold-constrained* and have low *local fractal dimension* (LFD). In other words, we assume that the dataset is embedded in a D-dimensional space, but that the data only occupy a d-dimensional manifold, where $d \ll D$. While we sometimes use Euclidean notions to describe the geometric and topological properties of the clusters and manifold, CLAM and CAKES do not rely on such notions; they serve merely as convenient and intuitive vocabulary to discuss the underlying mathematics. CAKES exploits the low LFD of such datasets to accelerate search. We define LFD at some length scale around a point in the dataset as:

$$\frac{\log\left(\frac{|B_X(q,r_1)|}{|B_X(q,r_2)|}\right)}{\log\left(\frac{r_1}{r_2}\right)} \tag{2.1}$$

where $B_X(q, r)$ is the set of points contained in the metric ball of radius r centered at a point q in the dataset $\mathbf{X}$. Intuitively, LFD measures the rate of change in the number of points in a ball of radius r around a point q as r increases. When the vast majority of points in the dataset have low ($\ll D$) LFD, we can simply say that the dataset has low LFD. We stress that this concept differs from the *embedding dimension* of a dataset. To illustrate the difference, consider the SILVA 18S rRNA dataset which contains genomic sequences with unaligned lengths of up to 3,718 base pairs and aligned length of 50,000 base pairs. Hence, the *embedding dimension* of this dataset is at least 3,718 and at most 50,000. However, physical constraints (namely, biological evolution and biochemistry) constrain the data to a lower-dimensional manifold within this space. LFD is an approximation of the dimensionality of that lower-dimensional manifold in the “vicinity” of a given point. Figure 2 illustrates this concept on a variety of datasets, showing how real datasets uphold the manifold hypothesis.

2.1. Clustering. We define a *cluster* as a set of points with a *center* and a *radius*. The center is the geometric median of the points (or a smaller sample of the points) in the cluster, and so it is a real data point. The radius is the maximum distance from the center to any point in the cluster. Each non-leaf cluster has two child clusters in much the same way that a node in a binary tree has two child nodes. Note that clusters can have overlapping volumes and, in such cases, points in the overlapping volume are assigned to exactly one of the overlapping clusters. As a consequence, a cluster can be a proper subset of the metric ball at the same center and radius, i.e. $C(c, r) \subset B_X(c, r)$.

Hereafter, when we refer to the LFD of a cluster, it is estimated at the length scale of the cluster radius and half that radius. This allows us to rewrite Definition 2.1 as $\log_2\left(\frac{|C(c,r)|}{|C(c,\frac{r}{2})|}\right)$

where $|C(c,r)|$ is the cardinality of the cluster C with center c and radius r, and $C(c,\frac{r}{2})$ is the set of points in C which are no more than a distance $\frac{r}{2}$ from c, i.e. $C(c,\frac{r}{2}) = \{p : p \in C \wedge f(c,p) \leq \frac{r}{2}\}$.

The *metric entropy* $\mathcal{N}_r(X)$ for some radius r was defined, in [37], as the minimum number of clusters of a uniform radius r needed to cover the data. In this paper, where the clustering is hierarchical rather than flat, we define the metric entropy $\mathcal{N}_{\hat{r}}(X)$ of a dataset X as the number of leaf clusters in the tree where $\hat{r}$ is the mean radius of all leaf clusters.

We start by performing a divisive hierarchical clustering on the dataset using CLAM. The procedure is similar to that outlined in CHESS [18], but with better selection of poles for partitioning (see Algorithm 2.1) and depth-first reordering of the dataset (see Section 2.1.2).

2.1.1. Building the Tree. CLAM builds a binary tree of clusters using a divisive hierarchical clustering algorithm. For a cluster C with $|C|$ points, we begin by taking a random sample of $\sqrt{|C|}$ of its points, and computing pairwise distances between all points in this sample. Using these distances, we compute the *geometric median* of this sample; in other words, we find the point which minimizes the sum of distances to all other points in the sample. This geometric median is the center of C.

The *radius* of C is the maximum distance from the *center* to any other point in C. The point which is responsible for that radius (i.e., the furthest point from the center) is designated the *left pole* and the point which is furthest from the left pole is designated the *right pole*. We then partition the cluster into a *left child* and a *right child*, where the left child contains all points in the cluster which are closer to the left pole than to the right pole, and the right child contains all points in the cluster which are closer to the right pole than to the left pole. Without loss of generality, we assign to the left child those points which are equidistant from the two poles. Starting from a root cluster containing the entire dataset, we repeat this procedure until each leaf contains only one datum, or we meet some other user-specified stopping criteria, for example, minimum cluster radius, minimum cluster cardinality, maximum tree depth, etc. This process is described in Algorithm 2.1. During the partitioning process, we also compute (and cache) the LFD of each cluster using Equation 2.1.

Note that Algorithm 2.1 does not necessarily produce a balanced tree. In fact, for real datasets, we expect anything but a balanced tree; the varying sampling density in different regions of the manifold and the low dimensional "shape" of the manifold itself will cause it to be unbalanced. The only case in which we would expect a balanced tree is if the dataset were uniformly distributed, e.g. in a d-dimensional hyper-cube. In this sense, the imbalance in the tree is a feature, not a bug, as it reflects the underlying structure of the data.

2.1.2. Depth-First Reordering. In CHESS, each cluster stored a list of indices into the dataset. This list was used to retrieve the clusters' points during search. Although this approach allowed us to retrieve the points in constant time, its memory cost was prohibitively high. With a dataset of cardinality n and each cluster storing a list of indices for its points, we stored a total of n indices at each depth in the tree. Assuming a balanced tree, and thus $\mathcal{O}(\log n)$ depth, this approach had a memory overhead of $\mathcal{O}(n \log n)$. In this work, we introduce a new approach wherein, after building the cluster tree, we reorder the dataset so that points are stored in a depth-first order. Then, within each cluster, we need only store its *cardinality* and an *offset* to access its points from the dataset, based on a useful invariant. The root cluster has

Algorithm 2.1 Partition(C, *criteria*)

```
Require: $C$, a cluster
Require: $criteria$, user-specified stopping criteria
  $seeds \Leftarrow$ random sample of $\lceil \sqrt{|C|} \rceil$ points from $C$
  $c \Leftarrow$ geometric median of $seeds$
  $l \Leftarrow \arg\max f(c, x) \ \forall \ x \in C$
  $r \Leftarrow \arg\max f(l, x) \ \forall \ x \in C$
  $L \Leftarrow \{x \mid x \in C \wedge f(l, x) \leq f(r, x)\}$
  $R \Leftarrow \{x \mid x \in C \wedge f(r, x) < f(l, x)\}$
  if $|L| > 1$ and $L$ satisfies $criteria$ then
      Partition($L$, $criteria$)
  end if
  if $|R| > 1$ and $R$ satisfies $criteria$ then
      Partition($R$, $criteria$)
  end if
```

an offset of zero and a cardinality equal to the number of points in the dataset. A left child has the same offset its parent, and the corresponding right child has an offset equal to the left child's offset plus the left child's cardinality. With no additional memory cost nor time cost for retrieving points during search, depth-first reordering offers the same time complexity as CHESS with $\mathcal{O}(n)$ space.

2.1.3. Complexity. The asymptotic complexity of Partition is the same as described in [18]. By using an approximate partitioning with a $\sqrt{n}$ sample, we achieve $\mathcal{O}(n)$ cost of partitioning and $\mathcal{O}(n \log n)$ cost of building the tree. This is a significant improvement over exact partitioning and tree-building, which cost $\mathcal{O}(n^2)$ and $\mathcal{O}(n^2 \log n)$ respectively.

2.2. The Search Problem.

Given Algorithm 2.1, we can now formally pose the k-NN and ρ-NN search problems.

Given a query q, along with a distance function f defined on a dataset $\mathbf{X}$, we define the k-NN search problem, which aims to find the k closest points to q in $\mathbf{X}$; in other words, k-NN search aims to find the set H such that $|H| = k$ and $H = B_X(q, \rho_k)$ where $\rho_k = \max\{f(q, p) \ \forall \ p \in H\}$ is the distance from q to the k^{th} nearest neighbor in $\mathbf{X}$. We also have the ρ-NN search problem, which aims to find the all points in $\mathbf{X}$ that are no more than a distance ρ from q: the set $H = B_X(q, \rho) = \{x \in \mathbf{X} : f(q, x) \leq \rho\}$.

Given a cluster C, let c be its center and r be its radius. Our ρ-NN and k-NN search algorithms make use of the following properties, as illustrated in Figure 1a.

- $\delta = f(q, c)$, the distance from the query to the cluster center c.
- $\delta^+ = \delta + r$, the distance from the query to the theoretically farthest point in C.
- $\delta^- = \max(0, \delta - r)$, the distance from the query to the theoretically closest point in C.

We define a *singleton* as a cluster which either contains a single point (i.e., has cardinality 1) or which contains only duplicates of the same point. A singleton clearly has zero radius, and so $\delta = \delta^- = \delta^+$. Hence, we overload the above notation to also refer to the distance from a query to an individual point.

2.3. ρ-Nearest Neighbors Search. We conduct ρ-NN search as described in [18], but with the following improvement: when a cluster overlaps with the query ball, instead of always proceeding to search both of its children, we proceed only with those children which might contain points in the query ball.

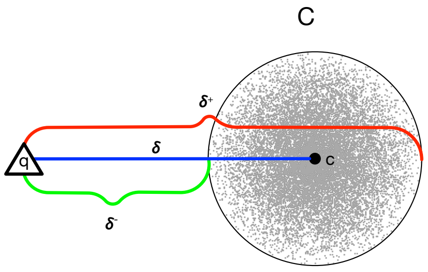

(a) δ, δ^+, and δ^- for a cluster C and a query q.

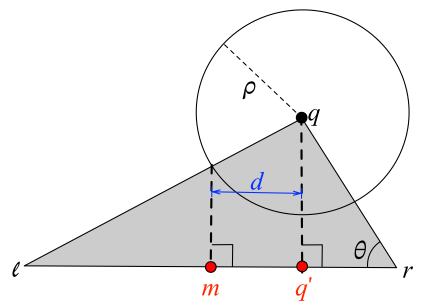

(b) The geometry of a query ball overlapping with a cluster and either one or both of its children. Here, l is the left pole, r is the right pole, and q is the query. Other points and distances are described in the text.

Figure 1: CAKES uses geometric properties of clusters.

To determine whether both children can contain points in the query ball, we consider Figure 1b. Here, we overload the notation for $\overline{xy}$ to refer both to the line segment joining points x and y as well as to the length of that line segment.

Let q denote the query, ρ denote the search radius, and l and r denote the cluster's left and right poles respectively (see Section 2.1.1). Without loss of generality, we assume that $\overline{qr} \leq \overline{ql}$. Now let q' be the projection of q onto $\overline{lr}$, m be the midpoint of $\overline{lr}$, and d be the distance from q' to m. As a consequence of how we assign a point in the parent cluster to the left child in Algorithm 2.1, if $\rho < d$, then the left child cannot contain points inside the query ball. In such a case we proceed to search only the right child. Otherwise, we proceed with both children.

To check whether $d \leq \rho$, we note that $d = \overline{mq'} = \overline{mr} - \overline{q'r} = \frac{\overline{lr}}{2} - \overline{q'r}$. Let θ denote $\angle lrq$, as shown in Figure 1b. By the Law of Cosines on $\triangle lrq$, we have that $\cos(\theta) = \frac{\overline{lr}^2 + \overline{qr}^2 - \overline{ql}^2}{2 \cdot \overline{lr} \cdot \overline{qr}}$. Since $\triangle rqq'$ is a right triangle, we also have that $\cos(\theta) = \frac{\overline{q'r}}{\overline{qr}}$. Combining the previous two equations and solving for $\overline{q'r}$, we have that $\overline{q'r} = \frac{\overline{qr}^2 + \overline{lr}^2 - \overline{ql}^2}{2 \cdot \overline{lr}}$. Substituting for $\overline{q'r}$ in the equation for d, we have that $d = \frac{\overline{lr}}{2} - \frac{\overline{qr}^2 + \overline{lr}^2 - \overline{ql}^2}{2 \cdot \overline{lr}} = \frac{\overline{ql}^2 - \overline{qr}^2}{2 \cdot \overline{lr}}$.

Thus, $d \leq \rho \iff (\overline{ql} + \overline{qr})(\overline{ql} - \overline{qr}) \leq 2 \cdot \overline{lr} \cdot \rho$. Note, in particular, that this only requires distances between real points, and so it can be used with any distance function, even when q' and m are not real points or cannot be imputed from the data.

To perform ρ-NN search, we first perform a coarse *tree-search*, as outlined in Algorithm 2.2, to find the leaf clusters which overlap with the query ball or any clusters which lie entirely within the query ball. Then, for all such clusters, we perform a finer-grained *leaf-search*, as outlined in Algorithm 2.3, to find all points which are no more than a distance ρ from the query. The asymptotic complexity of ρ-NN is the same as in [18] and shown in Equation 2.2.

Algorithm 2.2 tree-search(C, q, ρ)

```
Require: $C$, a cluster
Require: $q$, a query
Require: $\rho$, a search radius
  if $C$ is a leaf or $\delta_C^+ \leq \rho$ then
      return $\{C\}$
  else
      $[l, r] \Leftarrow$ poles of $C$
      $[L, R] \Leftarrow$ children of $C$
      if $\overline{ql} < \overline{qr}$ then
          $[r, l] \Leftarrow [l, r]$
          $[R, L] \Leftarrow [L, R]$
      end if
      if $(\overline{ql} + \overline{qr})(\overline{ql} - \overline{qr}) \leq 2 \cdot \overline{lr} \cdot \rho$ then
          return tree-search($L, q, \rho$) $\cup$ tree-search($R, q, \rho$)
      else
          return tree-search($R, q, \rho$)
      end if
  end if
```

Algorithm 2.3 leaf-search(S, q, ρ)

```
Require: $S$, a set of clusters
Require: $q$, a query
Require: $\rho$, a search radius
  $H \Leftarrow \emptyset$, a set of hits
  for $C \in S$ do
      if $\delta_C^+ \leq \rho$ then
          $H \Leftarrow H \cup \{C\}$
      else
          for $p \in C$ do
              if $f(p, q) \leq \rho$ then
                  $H \Leftarrow H \cup \{p\}$
              end if
          end for
      end if
  end for
  return $H$
```

Algorithm 2.4 ρ-NN-search($root$, q, ρ)

```
Require: $root$, the root cluster
Require: $q$, a query
Require: $\rho$, a search radius
  $S \Leftarrow$ tree-search($root$, $q$, $\rho$)
  $H \Leftarrow$ leaf-search($S$, $q$, $\rho$)
  return $H$
```

$$\mathcal{O}\left(\underbrace{\log \overbrace{\mathcal{N}_{\hat{r}}(X)}^{\text{metric entropy}}}_{\text{tree-search}} + \underbrace{\overbrace{|B_X(q,\rho)|}^{\text{output size}} \overbrace{\left(\frac{\rho + 2\cdot\hat{r}}{\rho}\right)^d}^{\text{scaling factor}}}_{\text{leaf-search}} \right) \tag{2.2}$$

where $\hat{r}$ is the *mean* radius of leaf clusters, $\mathcal{N}_{\hat{r}}(X)$ is the metric entropy at that radius, $B_X(q, \rho)$ is a ball of radius ρ around the query q, and d is the LFD around the query at the length scale of ρ and $\rho + 2 \cdot \hat{r}$.

From Algorithm 2.4, we have that $H = B_X(q, \rho)$, and so ρ-NN search performance scales linearly with the size of the output set and exponentially with the LFD around the query. While one might worry that the exponential scaling factor would dominate, the manifold hypothesis suggests that the LFD of real-world datasets is typically very low, and so this algorithm actually scales sub-linearly with the cardinality of the dataset.

2.4. k-Nearest Neighbors Search. In this section, we present three novel algorithms for exact k-NN search: Repeated ρ-NN, Breadth-First Sieve, and Depth-First Sieve.

In these algorithms, we use H, for *hits*, to refer to the data structure which stores the closest points to the query found so far, and Q to refer to the data structure which stores the clusters and points which are still in contention for being one of the k nearest neighbors.

2.4.1. Repeated ρ-NN. In this algorithm, we perform ρ-NN search starting with a small search radius, and repeatedly increasing the radius until $|H| \geq k$.

Let the search radius r be equal to the radius of the root cluster divided by the cardinality of the dataset. We perform tree-search with radius r. If no clusters are found, then we double r and perform tree-search again, repeating until we find at least one cluster. Let Q be the set of clusters returned by the first tree-search which returns at least one cluster.

Now, so long as $\sum_{C \in Q} |C| < k$, we continue to perform tree-search, but instead of doubling r on each iteration, we multiply it by a factor determined by the LFD in the vicinity of the query ball. In particular, we increase the radius by a factor of

$$\min \left(2, \left(\frac{k}{\sum_{C \in Q} |C|} \right)^{\mu^{-1}} \right) \tag{2.3}$$

where μ is the harmonic mean of the LFD of the clusters in Q. We use the harmonic mean to ensure that μ is not dominated by outlier clusters with very high LFD. We cap the radial increase at 2 to ensure that we do not increase the radius too quickly in any single iteration.

Intuitively, the factor by which we increase the radius should be *inversely* related to the number of points found so far. When the LFD at the radius scale from the previous iteration is high, this suggests that the data are densely populated in that region. Thus, a small increase in the radius would likely encounter many more points, so a smaller radial increase would suffice to find k neighbors. Conversely, when the LFD at the radius scale from the previous iteration is low, this suggests that the data are sparsely populated in that region. In such a region, a small increase in the radius would likely encounter vacant space, so a larger radial increase is needed. Thus, the factor of radius increase should also be *inversely* related to the LFD.

Once $\sum_{C \in Q} |C| \geq k$, we are guaranteed to have found at least k neighbors, and so we can stop increasing the radius. We perform ρ-NN search with this radius and return the k nearest neighbors.

Algorithm 2.5 Repeated ρ-NN($root$, q, k)

```
Require: $root$, the root cluster
Require: $q$, a query
Require: $k$, the number of neighbors to find
  $r \Leftarrow radius$ of the $root$ cluster
  $r \Leftarrow \frac{r}{|root|}$
  loop
      $Q \Leftarrow$ tree-search($root$, $q$, $r$)
      if $Q \neq \emptyset$ then
          break
      end if
      $r \Leftarrow 2 \cdot r$
  end loop
  loop
      if $\sum_{C \in Q} |C| >= k$ then
          break
      end if
      $\mu \Leftarrow \frac{|S|}{\sum_{C \in Q} \frac{1}{LFD(C)}}$
      $r \Leftarrow r \cdot \min \left( 2, \left( \frac{k}{\sum_{C \in Q} |C|} \right)^{\mu^{-1}} \right)$
      $S \Leftarrow$ tree-search($root$, $q$, $r$)
  end loop
  $H \Leftarrow$ sort($\rho$-NN-search($root$, $q$, $r$))
  return $H[..k]$
```

2.4.2. Complexity of Repeated ρ-NN. The complexity bounds for Repeated ρ-NN rely on the assumption that the query point is sampled from the same distribution as the rest of the data or, in other words, that it arises from the same generative process as the rest of the dataset. Given the uses of k-NN search in practice, this assumption is reasonable. From this assumption, we can infer that the LFD near the query does not differ significantly from the (harmonic) mean of the LFDs of clusters near the query at the scale of the distance from the query to the k^{th} nearest neighbor.

We find it useful to adopt the terminology used in [18] and [37], and address *tree-search* and *leaf-search* separately. Tree-search refers to the process of identifying clusters which have overlap with the query ball, or in other words, clusters which might contain one of the k nearest neighbors. Leaf-search refers to the process of identifying the k nearest neighbors among the points in the clusters identified by tree-search.

In [18], we showed that the complexity of tree-search is $\mathcal{O}(\log \mathcal{N}_{\hat{r}}(X))$, where $\mathcal{N}_{\hat{r}}(X)$ is the metric entropy of the dataset X at a radius $\hat{r}$. To adjust this bound for Repeated ρ-NN, we must estimate the number of iterations of tree-search (Algorithm 2.2) needed to find a radius that guarantees at least k neighbors.

Based on the assumption that the LFD near the query does not differ significantly from that of nearby clusters, Equation 2.3 suggests that in the expected case, we need only two iterations of tree-search to find k neighbors: one iteration to find at least one cluster, and the one more to find enough the k neighbors. Since this is a constant factor, complexity of tree-search for Repeated ρ-NN is the same as that of ρ-NN search, i.e. $\mathcal{O}\big(\log \mathcal{N}_{\hat{r}}(X)\big)$.

To determine the asymptotic complexity of leaf-search, we must estimate $\sum_{C \in Q} |C|$, the total cardinality of the clusters returned by tree-search. Since we must examine every point in each such clusters, time complexity of leaf-search is linear in $\sum_{C \in Q} |C|$. Let ρ_k be the distance from the query to the k^{th} nearest neighbor. Then, we see that Q is expected to be the set of clusters which overlap with a ball of radius ρ_k around the query. We can estimate this region as a ball of radius $\rho_k + 2\hat{r}$, where $\hat{r}$ is the mean radius of the clusters in Q.

The work in [37] showed that $\sum_{C \in S} |C| \leq \gamma \, |B(q, \rho_k)| \left(\frac{\rho_k + 2 \cdot \hat{r}}{\rho_k}\right)^d$, where γ is a constant. By definition of ρ_k, we have that $|B(q, \rho_k)| = k$. Thus, $\sum_{C \in S} |C| \leq \gamma k \left(1 + 2 \cdot \frac{\hat{r}}{\rho_k}\right)^d$. However, an estimate for ρ_k is still needed. For this, we once again rely on the assumption that the query is drawn from the same distribution as the rest of the data, and thus the LFD at the query point is not significantly different from the LFD of nearby clusters. We let $\hat{d}$ be the (harmonic) mean LFD of the clusters in Q. While ordinarily we compute LFD by comparing cardinalities of two balls with two different radii centered at *the same* point, in order to estimate ρ_k, we instead compare the cardinality of a ball *around the query* of radius ρ_k to the mean cardinality, $|\hat{C}|$, of clusters in Q at a radius equal to the mean of their radii, $\hat{r}$. We justify this approach by noting that, since the query is from the same distribution as the rest of the data, we could move from the query to the center of one of the nearby clusters without significantly changing our estimate of the LFD. By Equation 2.1, $\hat{d} = \frac{\log \frac{|\hat{C}|}{k}}{\log \frac{\hat{r}}{\rho_k}}$. We can rearrange this equation to get $\frac{\hat{r}}{\rho_k} = \left(\frac{|\hat{C}|}{k}\right)^{\hat{d}^{-1}}$. Using this to simplify the term for leaf-search in Equation 2.2, we get $k \left(1 + 2 \cdot \left(\frac{|\hat{C}|}{k}\right)^{\hat{d}^{-1}}\right)^d$.

In addition, by our assumption that the LFD at the query is not significantly different from the LFD of nearby clusters, we have that $\hat{d} \approx d$. By combining the bounds for tree-search and leaf-search, we see that Repeated ρ-NN has an asymptotic complexity of

$$\mathcal{O}\Bigg(\underbrace{\log \overbrace{\mathcal{N}_{\hat{r}}(X)}^{\text{metric entropy}}}_{\text{tree-search}} + \underbrace{\overbrace{k}^{\text{output size}} \overbrace{\left(1 + 2 \cdot \left(\frac{|\hat{C}|}{k}\right)^{d^{-1}}\right)^{d}}^{\text{scaling factor}}}_{\text{leaf-search}} \Bigg) \tag{2.4}$$

where $\mathcal{N}_{\hat{r}}(X)$ is the metric entropy of the dataset, d is the LFD of the dataset, and k is the number of nearest neighbors. We note that the scaling factor should be close to 1 unless fractal dimension is highly variable in the region around the query (i.e. if $\hat{d}$ differs significantly from d).

2.4.3. Breadth-First Sieve.

This algorithm performs a breadth-first traversal of the tree, pruning clusters by using a modified version of the QuickSelect algorithm [15] at each level.

We begin by letting Q be a set of 3-tuples (p, δ_p^+, m), where p is either a cluster or a point, δ_p^+ is the δ^+ of p as illustrated in Figure 1a, and m is the multiplicity of p in Q. During the breadth-first traversal, for every cluster C we encounter, we add $(C, \delta_C^+, |C| - 1)$ and $(c, \delta_c, 1)$ to Q, where c is the center of C. Recall that by the definitions of δ and δ^+ given in Section 2.2, since c is a point, $\delta_C = \delta_c = \delta_c^+ = \delta_c^-$.

We then use the QuickSelect algorithm, modified to account for multiplicities and to reorder Q in-place, to find the element in Q with the k^{th} smallest δ^+; in other words, we find τ, the smallest δ^+ in Q such that $|B_X(q, \tau)| \geq k$. Since this step may require a binary search for the correct pivot element to find τ and reordering with a new pivot takes linear time in the size of the input list, this version of QuickSelect has $\mathcal{O}(|Q| \log |Q|)$ time complexity.

We then remove from Q any element for which $\delta^- > \tau$ because such elements cannot contain (or be) one of the k nearest neighbors. Next, we remove all leaf clusters from Q and add their points to Q instead. Finally, we replace all remaining clusters in Q with the pairs of 3-tuples corresponding to their child clusters.

We continue this process until Q no longer contains any clusters. We then use the QuickSelect algorithm one last time to reorder Q, find τ, and return the k nearest neighbors.

This process is described in Algorithm 2.6.

Algorithm 2.6 Breadth-First Sieve($root$, q, k)

```
Require: $root$, the root cluster
Require: $q$, a query
Require: $k$, the number of neighbors to find
  $c \Leftarrow center$ of $root$
  $Q \Leftarrow \{ (root, \delta^+_{root}, |root| - 1), (c, \delta_{root}, 1) \}$
  loop
      if $k = \sum_{(\_,\_,m) \in Q} m$ then
          break
      end if
      $\tau \Leftarrow$ QuickSelect($Q$, $k$)
      for $(p, \delta^+_p, m) \in Q$ do
          if $\delta^-_p > \tau$ then
              $Q \Leftarrow Q \setminus \{(p, \delta^+_p, m)\}$
          end if
      end for
      for $(p, \delta^+_p, m) \in Q$ do
          $Q \Leftarrow Q \setminus \{(p, \delta^+_p, m)\}$
          if $p$ is a point then
              continue
          else if $p$ is a leaf then
              for $c \in p$ do
                  $Q \Leftarrow Q \cup \{(c, \delta_c, 1)\}$
              end for
          else
              $[L, R] \Leftarrow$ children of $p$
              $Q \Leftarrow Q \cup \{(L, \delta^+_L, |L| - 1), (L_c, \delta_L, 1)\}$
              $Q \Leftarrow Q \cup \{(R, \delta^+_R, |R| - 1), (R_c, \delta_R, 1)\}$
          end if
      end for
  end loop
  return $Q$
```

Algorithm 2.7 Depth-First Sieve($root$, q, k)

```
Require: $root$, the root cluster
Require: $q$, a query
Require: $k$, the number of neighbors to find
  $Q \Leftarrow [root]$, a min-priority queue by $\delta^-$
  $H \Leftarrow []$, a max-priority queue by $\delta$
  while $|H| < k$ or $H.peek.\delta \geq Q.peek.\delta^-$ do
      while $\neg(Q.peek$ is a leaf$)$ do
          $C \Leftarrow Q.pop$, the closest cluster
          $[L, R] \Leftarrow$ children of $C$
          $Q.push(L)$
          $Q.push(R)$
      end while
      $leaf \Leftarrow Q.pop$
      for $p \in leaf$ do
          $H.push(p)$
      end for
      while $|H| > k$ do
          $H.pop$
      end while
  end while
  Return $H$
```

2.4.4. Depth-First Sieve.

This algorithm performs a depth-first traversal of the tree and uses two priority queues to track clusters and hits.

Let Q be a min-queue of clusters prioritized by δ^- and H be a max-queue (with capacity k) of points prioritized by δ. Q starts containing only the root cluster while H starts empty. So long as H is not full or the top priority element in H has δ greater than or equal to the top priority element in Q, we take the following steps:

- While the top-priority element is not a leaf, remove it from Q and add its children to Q.
- Remove the top-priority element (a leaf) from Q and add all its points to H.
- If H has more than k points, remove points from H until $|H| = k$.

This process is described in Algorithm 2.7. It terminates when H is full and the top priority element in H has δ less than the top priority element in Q, i.e., the theoretically closest point left to be considered in Q is farther from the query than the k^{th} nearest neighbor in H. This leaves H containing exactly the k nearest neighbors to the query.

Note that this algorithm is not truly a depth-first traversal of the tree in the classical sense, because we use Q to prioritize which branch of the tree we descend into. Indeed, we expect this algorithm to often switch which branch of the tree is being explored at greater depth.

2.4.5. Complexity of Sieve Methods.

Due to their similarity, we combine the complexity analyses of both Sieve methods. For these methods we again use the terminology of tree-search and leaf-search. Tree-search navigates the cluster tree and adds clusters to Q. Leaf-search exhaustively searches some of the clusters in Q to find the k nearest neighbors.

We start with the assumption that the LFD near the query does not differ significantly from that of nearby clusters, and we consider leaf clusters with cardinalities near k. Let d be the LFD in this region. Then the number of leaf-clusters in Q is bounded above by $2d$, e.g. we could have a cluster overlapping the query ball at each end of each of $\lceil d \rceil$ mutually-orthogonal axes. In the worst-case scenario for tree-search, these leaf clusters would all come from different branches of the tree, and so tree-search looks at $2 \cdot \lceil d \rceil \cdot \log \mathcal{N}_{\hat{r}}(X)$ clusters. Thus, the asymptotic complexity is $\mathcal{T} := \mathcal{O}\big(\lceil d \rceil \cdot \log \mathcal{N}_{\hat{r}}(X)\big)$. For leaf-search, the output size and scaling factor are the same as in Repeated ρ-NN, and so the asymptotic complexity is $\mathcal{L} := \mathcal{O}\left(k \cdot \left(1 + 2 \cdot \left(\frac{|\hat{C}|}{k}\right)^{d^{-1}}\right)^{d}\right)$.

The asymptotic complexity of Breadth-First Sieve is dominated by the QuickSelect algorithm to calculate τ. Since this method is log-linear in the length of Q, and Q contains the clusters from tree-search and the points from leaf-search, we see that the asymptotic complexity is:

$$\mathcal{O}\Big((\mathcal{T} + \mathcal{L}) \log(\mathcal{T} + \mathcal{L})\Big). \tag{2.5}$$

For Depth-First Sieve, since we use two priority queues, the asymptotic complexity is dominated by the priority queue operations. Thus, the complexity is:

$$\mathcal{O}\Big(\mathcal{T} \log \mathcal{T} + \mathcal{L} \log k\Big). \tag{2.6}$$

2.5. Auto-Tuning. We perform some simple auto-tuning to select the optimal k-NN algorithm to use with a given dataset. We start by taking the center of every cluster at a low depth, (e.g. 10), in the cluster tree as a query. This gives us a small, representative sample of the dataset. Using these clusters' centers as queries, and a user-specified value of k, we record the time taken for k-NN search on the sample using each of the three algorithms described in Section 2.4. We select the fastest algorithm over all the queries as the optimal algorithm for that dataset and value of k. Note that even though we select the optimal algorithm based on use with some user-specified value of k, we still allow search with any value of k.

2.6. Synthetic Data. Based on our asymptotic complexity analyses, we expect CAKES to perform well on datasets with low LFD, and for its performance to scale sub-linearly with the cardinality of the dataset. To test this hypothesis, we use some datasets from the ANN-benchmarks suite [3] and synthetically augment them to generate similar datasets with exponentially larger cardinalities. We do the same with a large random dataset of uniformly distributed points in a hypercube. We then compare the performance of CAKES to that of other algorithms on the original datasets and the synthetically augmented datasets.

To elaborate on the augmentation process, we start with an original dataset from the ANN-benchmarks suite. Let X be the dataset, d be its dimensionality, ϵ be a user-specified noise level, and m be a user-specified integer multiplier. For each datum $x \in X$, we create $m - 1$ new data points within a distance $\epsilon \cdot ||x||$ of x where $||x||$ is the Euclidean distance from x to the origin. We construct a random vector r of d dimensions in the hyper-sphere of radius ϵ centered at the origin. We then add r to x to get a new point x'. Since $||r|| \leq \epsilon$, we have that $||x - x'|| \leq \epsilon$ (i.e., x' is within a distance ϵ of x). This produces a new dataset X' with $|X'| = m \cdot |X|$. This augmentation process preserves the topological structure of the original dataset, but increases its cardinality by a factor of m, allowing us to isolate the effect

Table 1: Datasets used in benchmarks.

Dataset	Distance	Cardinality	Dimensionality
Fashion-Mnist	Euclidean	60,000	784
Glove-25	Cosine	1,183,514	25
Sift	Euclidean	1,000,000	128
Random	Euclidean	1,000,000	128
SILVA	Levenshtein	2,224,640	3,712 - 50,000
RadioML	Dynamic Time Warping	97,920	1,024

of cardinality on search performance from that of other factors such as dimensionality, choice of metric, or the topological structure of the dataset.

3. Datasets And Benchmarking.

3.1. ANN-Benchmark Datasets. We benchmark on a variety of datasets from the ANN-benchmarks suite [2]. Table 1 summarizes these datasets. The benchmarks for Fashion-Mnist, Glove-25, Sift, and Random (and for their synthetic augmentations) were conducted on an Amazon AWS (EC2) `r6i.16xlarge` instance, with a 64-core Intel Xeon Platinum 8375C CPU 2.90GHz processor, 512GB RAM. This is the same configuration used in [2]. The OS kernel was Ubuntu 22.04.3-Ubuntu SMP. The Rust compiler was Rust 1.72.0, and the Python interpreter version was 3.9.16. The benchmarks for SILVA and RadioML were conducted on an Intel Xeon E5-2690 v4 CPU @ 2.60GHz with 512GB RAM. The OS kernel was Manjaro Linux 5.15.130-1-MANJARO. The Rust compiler was Rust 1.72.0, and the Python interpreter version was 3.9.16.

3.2. Random Datasets and Synthetic Augmentations. In addition to benchmarks on datasets from the ANN-Benchmarks suite, we also benchmarked on synthetic augmentations of these real datasets, using the process described in 2.6. In particular, we use a noise tolerance $\epsilon = 0.01$ and explore the scaling behavior as the cardinality multiplier (referred to as "Multiplier" in Table 2) increases. We also benchmarked on purely randomly-generated datasets of various cardinalities. For this, we used a base cardinality of 1,000,000 and a dimensionality of 128 to match the Sift dataset; hereafter, we refer to the random dataset with cardinality 1,000,000 and dimensionality 128 as "Random." This benchmark allows us to isolate the effect of a manifold structure (which we expect to be absent in a purely random dataset) on the performance of the CAKES' algorithms.

3.3. SILVA 18S. To demonstrate CAKES with a more exotic distance function, we also benchmarked on the SILVA 18S ribosomal RNA dataset [29]. This dataset contains ribosomal RNA sequences of 2,224,640 genomes with an aligned length of 50,000 letters. We held out a set of 1,000 random sequences from the dataset to use as queries for benchmarking. We use Levenshtein [23] distance on the unaligned sequences to build the tree and to perform k-NN search. Since this dataset contains many redundant, i.e. nearly identical, sequences, we used a maximum tree-depth of 128 as a partition criterion in Algorithm 2.1.

3.4. Radio ML. As another example of an exotic distance function, we benchmarked CAKES on the RadioML dataset [28]. The RadioML dataset contains samples of synthetically generated signal captures of different modulation modes over a range of SNR levels. Specifically, it comprises 24 modulation modes at 26 different signal-to-noise ratio (SNR) levels ranging from -20 dB to 30 dB, with 4,096 samples at each combination of modulation mode and SNR level. Thus, it contains $24 \cdot 26 \cdot 4096 = 2,555,504$ samples in total. Each sample is a 1,024-dimensional complex-valued vector, representing a signal capture (a time-series of complex-valued numbers). We used a subset of this dataset, containing 97,920 samples at 10dB SNR and used the other 8,576 samples at 10dB SNR as a hold-out set of queries. We use Dynamic Time Warping [26] as the distance function for this dataset.

3.5. Other Algorithms. We benchmarked CAKES's algorithms against the state-of-the-art similarity search algorithms HNSW, ANNOY and FAISS-IVF, and two implementations of linear search. In particular, we use FAISS-Flat, a Python implementation of linear search, to provide ground-truth values for recall of HNSW, ANNOY, and FAISS-IVF. We use our own Rust implementation of linear search to provide ground-truth values for calculating recall of CAKES's algorithms. We plot the throughput of these two implementations of linear search as a reference point for all other algorithms in Figure 3.

4. Results.

4.1. Local Fractal Dimension of Datasets. Since the time complexity of CAKES algorithms scales with the LFD of the dataset, we examine the LFD of each dataset we used for benchmarks. Figure 2 illustrates the trends in LFD for Fashion-Mnist, Glove-25, Sift, Random, Silva 18S, and RadioML. The horizontal axis denotes depth in the cluster tree, and the vertical axis denotes the LFD of clusters at that depth. We plot lines for the 5^{th}, 25^{th}, 50th, 75^{th} and 95^{th} percentiles of LFD, as well as the minimum and maximum LFD at each depth. In order to have the plots best reflect the distribution of LFDs across the entire *dataset*, we count each cluster as many times as its cardinality. In other words, if, for some dataset, the 95^{th} percentile of LFD at depth 40 is 3, this means that 95% of the points in clusters at depth 40 belong to a cluster whose LFD is at most 3. Figure 2a shows the LFD by depth for Fashion-Mnist. We observe that until about depth 5, LFD is low, as the 95^{th} percentile (orange plotted line) is less than 4, and the median (red line) is just above 2. For depths 15 through 25, we observe that LFD increases, with the 95^{th} percentile (orange plotted line) slightly less than 6, and the median near 3. Finally, for depths 25 through the maximum depth, we observe that the LFD decreases again, as the 95^{th} percentile is between 3 and 4, and the median is less than 2.

Relative to Fashion-Mnist, Glove-25 has low LFD, as shown in Figure 2b. Percentile lines for Glove-25 are flatter and lower, indicating that the LFD is lower across the entire dataset, and that the LFD does not vary as much by depth. The 95^{th} percentile of LFD is less than 3 for all depths, and the median is less than 2 for all depths. Before depth 25, the 95^{th} percentile hovers near 2, and from depth 20 onward, it hovers near 3.5 before dipping sharply at the maximum depths. The median hovers near 1.5 for all depths.

Figure 2c shows the LFD by depth for Sift. Until about depth 5, the 95^{th} percentile is between 2 and 6. From about depth 5 through about depth 20, the 95^{th} percentile is greater than 6, even exceeding 8 near depth 10. From about depth 20 onward, the 95^{th} percentile is less than 6, and from about depth 30 onward, it is between 3 and 4. The median reaches its peak of about 5 at around depth 15, but hovers near 2 after about depth 30.

In contrast with Figure 2c, Figure 2f shows the LFD by depth for a random dataset with the same cardinality and dimensionality as those of Sift. We observe that the LFD starts as high as 20 (for all data) at depth 0. As shown by the needlepoint shape of the plot, the LFD for all clusters has a very narrow spread from depth 0 through depth 5. After depth 5, we begin to see a wider spread between the maximum and minimum LFD at each depth. All percentile lines seem to decrease linearly with depth. The LFD of approximately 20 at depth 0 (i.e. the root cluster) is what we expect for this random dataset. To elaborate, the distribution of points in such a dataset should reflect the curse of dimensionality, i.e. the fact that in high dimensional spaces, the minimum and maximum pairwise distances between any two points are approximately equal. As a result, the root cluster's radius r, which reflects the maximum distance between the center c and any other point, should not differ significantly from the distance between the center and its closest point. A consequence of this is that, with high probability, for every point in the root cluster, its distance from c is greater than $\frac{r}{2}$; in other words, $B_X(c, \frac{r}{2})$ contains only c while $B_X(c, r)$ contains the entire dataset. Given our definition of LFD in Equation 2.1, this means that the LFD of the root cluster is approximately $\log_2(\frac{|X|}{1}) = \log_2(1,000,000) \approx 20$, which is what we observe in Figure 2f.

Silva, as shown in Figure 2e, exhibits consistently low LFD. The 95th percentile is less than about 3 for all depths, hovering near 1 for depths 40 through 128. The median reaches its peak at 2 for about depth 10 and remains close to 0 for depths 40 through 128.

Relative to the other datasets, RadioML, as displayed in Figure 2d, exhibits high LFD. Notably, however, for the first approximately 15 depths, the 95th percentile and median LFD are very close to 0. Both percentiles increase sharply after depth 20, nearly reaching 16. LFD remains high even as depth increases, with the 95th percentile fluctuating between about 6 and 15 for depths about 20-40. It then spikes up again to about 10 at around depth 45 before decreasing linearly to 1 at depth 60. The median LFD follows a similar pattern of peaks and troughs, fluctuating between about 3 and 15 for depths 20-40, spiking at about depth 50 to 5, and then decreasing approximately linearly to 1 at depth 60. The inconsistency of LFD in the RadioML dataset suggests that it obeys the manifold hypothesis at some scales, but that it is not "scale free," as the LFD varies significantly by depth; this could be due to dense sampling or – as this is still a synthetic dataset – nonuniform generation of data. Silva, in contrast, appears to obey the manifold hypothesis at all scales.

4.2. Indexing and Tuning Time. For each of the ANN-benchmark datasets and the Random dataset, we report the time taken for each algorithm to build the index and to tune the hyper-parameters for these indices to achieve the highest possible recall. For the sake of brevity, these results are reported in the supplement.

4.3. Scaling Behavior and Recall. Figures 3a, 3b, and 3c show the scaling behavior of CAKES algorithms and existing algorithms on augmented versions of Fashion-Mnist under Euclidean distance, Glove-25 under cosine distance, and Sift under Euclidean distance. Figure 3f shows the scaling behavior of CAKES algorithms and existing algorithms on a completely randomly generated dataset with the same cardinality and dimensionality as Sift (1 million points in 128 dimensions). Figures 3e and 3d show the scaling behavior of CAKES on Silva

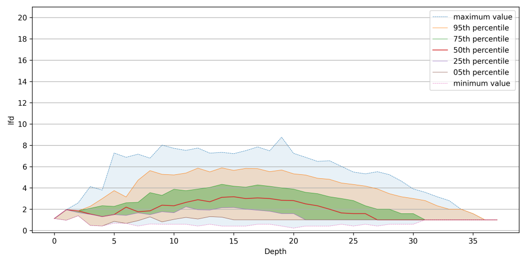

(a) Fashion-mnist

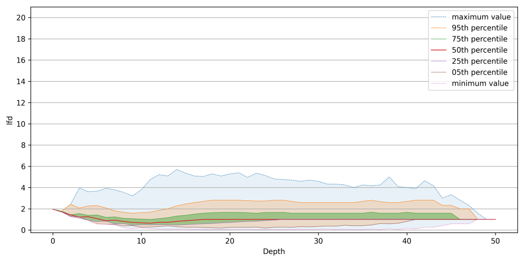

(b) Glove-25

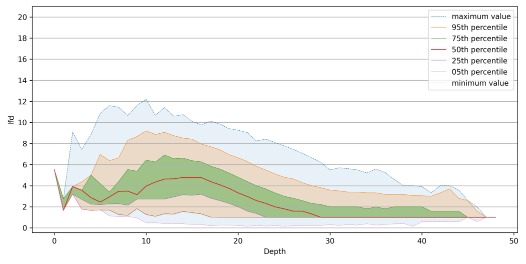

(c) Sift

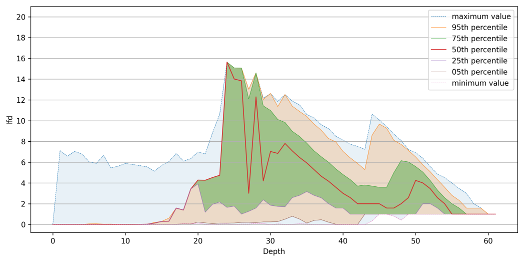

(d) RadioML

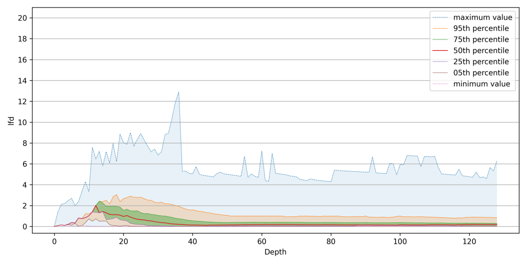

(e) Silva 18S

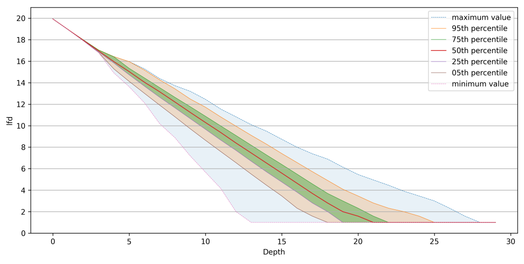

(f) A random dataset

Figure 2: Local fractal dimension vs. cluster depth across six datasets, grouped by decile of local fractal dimension and weighted by the cardinalities of the clusters. The last dataset is randomly generated.

and RadioML respectively. For these datasets, we took random sub-samples of the full datasets instead of augmenting them to higher cardinalities. The horizontal axis in each figure shows the cardinality of the dataset augmented with synthetic points (see Section 2.6). The left-most point on each line is at the cardinality of the original dataset. The vertical axis denotes throughput in queries per second. Both axes are on a logarithmic scale. In this section, we report results only for k-NN search with $k = 10$, but similar plots for $k = 100$ can be found in the Supplement. For HNSW and ANNOY, we report the recall for each measurement in the plots. For algorithms which exhibit recall greater than 0.9995, we do not report the recall in the plots, but we do report it in the tables below.

Table 2 show the throughput and recall of CAKES's algorithms at each augmented cardinality for Fashion-Mnist, Glove-25, Sift, and Random. Though the plots in Figure 3 present results for each of CAKES's three algorithms separately, the results in the CAKES column in these tables represent the fastest CAKES algorithm at that dataset and cardinality only. We used our auto-tuning approach (see Section 2.5) for each new tree (i.e. at each cardinality), and this approach was always able to select the fastest algorithm for each dataset at each cardinality. Since we also allow for tuning hyper-parameters for the other algorithms, and we allow for different sets of hyper-parameters at each cardinality, it is a fair comparison for these tables to only list the performance of the tuned CAKES algorithm. When reporting recall, we use $1.000*$ to denote that the recall is imperfect, but rounds to 1.000.

Figure 3 shows that for Fashion-Mnist, Glove-25, and Sift, as cardinality increases, the CAKES algorithms (Depth-First Sieve in blue, Repeated ρ-NN in green, and Breadth-First Sieve in purple) become faster than our Rust implementation of naïve linear search (in orange). Though we observe this trend, we note that the exact cardinality at which CAKES's algorithms overtake linear search differs by dataset. For Fashion-Mnist, CAKES begins outperforming linear search starting at a cardinality near 10^5, while for Glove-25 and Sift, this happens near 10^6 and 10^7 respectively. Which one of the three CAKES algorithms is fastest also differs by dataset. For Fashion-Mnist, Depth-First Sieve is consistently fastest, while for Glove-25, the fastest is Repeated ρ-NN, and for Sift, Breadth-First Sieve. On all three datasets, Depth-First Sieve and Breadth-First Sieve appear to have performance which is *constant* in the cardinality of the dataset. With Glove-25, Repeated ρ-NN exhibits similar constant scaling. We also observe that on these three datasets, for nearly all cardinalities, all three of the CAKES algorithms are faster than FAISS-Flat (in brown), and that at some cardinality, CAKES's algorithms become faster than FAISS-IVF (in pink). For Fashion-Mnist, CAKES becomes faster than FAISS-IVF near cardinality 10^5, whereas for Glove-25 and Sift, this happens near cardinality 10^7. On all three of these datasets, HNSW (in gray) and ANNOY (in yellow) are faster than CAKES's algorithms for all cardinalities; however, CAKES exhibits perfect or near-perfect recall on each dataset, while HNSW and ANNOY exhibit much lower recall, as shown in Table 1. While recall for CAKES's does *not* degrade with cardinality, recall for HNSW and ANNOY degrades with cardinality. At a cardinality multiplier as low as eight, HNSW and ANNOY have recall of 0.525 and 0.857 respectively for Fashion-Mnist, 0.607 and 0.832 for Glove-25, and 0.782 and 0.686 on Sift. In contrast, CAKES has perfect recall on Fashion-Mnist and Sift (where the distance function is a metric), and near-perfect recall on Glove-25 (cosine distance is not a metric).

In contrast with the results on the ANN Benchmark datasets reported above, with the Random dataset, as seen in Figure 3f, we observe performs quite slowly. As with the real datasets, HNSW and ANNOY are the fastest algorithms, and CAKES exhibits perfect recall at all cardinalities. HNSW and ANNOY exhibit *much* lower recall on this random dataset than on any of the ANN benchmark datasets; in particular, with a multiplier of 1, HNSW and ANNOY have recall as low as 0.060 and 0.028 respectively, as reported in Table 2.

For Silva and RadioML, we benchmarked only CAKES's algorithms because HNSW, ANNOY and FAISS support neither the required distance functions nor, in the case of RadioML, complex-valued data. Due to the massive sizes of these datasets and challenges in generating plausible augmentations, we took random sub-samples ranging up to the entirety of the dataset–rather than augmented versions of the dataset–to examine how performance scales with cardinality. With Silva, as shown in Figure 3e, we observe that for all algorithms, throughput initially seems to linearly decrease as cardinality increases, but that it seems to begin levelling off near cardinality 10^5. Until cardinality near 10^4, Depth-First Sieve is the fastest CAKES algorithm, but for larger cardinalities, Repeated ρ-NN is the fastest CAKES algorithm. For RadioML, as shown in Figure 3d, we observe that throughput declines nearly linearly, and that the three CAKES algorithms exhibit virtually indistinguishable performance. In particular, throughput of CAKES's algorithms is identical within three significant figures.

Table 2: Queries per second (QPS) and Recall vs naive linear search on the Fashion-Mnist, Glove-25, Sift and Random datasets. A recall value of 1.000∗ denotes imperfect recall that rounds to 1.000.

	Multiplier	hnsw		annoy		faiss-ivf		cakes	
		QPS	Recall	QPS	Recall	QPS	Recall	QPS	Recall
Fashion-Mnist	1	1.33×10^4	0.954	2.19×10^3	0.950	2.01×10^3	1.000*	2.17×10^3	1.000
	2	1.38×10^4	0.803	2.12×10^3	0.927	9.39×10^2	1.000*	1.14×10^3	1.000
	4	1.66×10^4	0.681	2.04×10^3	0.898	4.61×10^2	0.997	9.82×10^2	1.000
	8	1.68×10^4	0.525	1.93×10^3	0.857	2.26×10^2	0.995	1.18×10^3	1.000
	16	1.87×10^4	0.494	1.84×10^3	0.862	1.17×10^2	0.991	1.20×10^3	1.000
	32	1.56×10^4	0.542	1.85×10^3	0.775	5.91×10^1	0.985	1.16×10^3	1.000
	64	1.50×10^4	0.378	1.78×10^3	0.677	2.61×10^1	0.968	1.10×10^3	1.000
	128	1.49×10^4	0.357	1.66×10^3	0.538	1.33×10^1	0.964	1.04×10^3	1.000
	256	–	–	1.60×10^3	0.592	6.65×10^0	0.962	1.06×10^3	1.000
	512	–	–	1.83×10^3	0.581	3.56×10^0	0.949	1.04×10^3	1.000
Glove-25	1	2.28×10^4	0.801	2.83×10^3	0.835	2.38×10^3	1.000*	7.22×10^2	1.000*
	2	2.38×10^4	0.607	2.70×10^3	0.832	1.19×10^3	1.000*	5.75×10^2	1.000*
	4	2.50×10^4	0.443	2.61×10^3	0.839	6.19×10^2	1.000*	6.25×10^2	1.000*
	8	2.78×10^4	0.294	2.51×10^3	0.834	3.03×10^2	1.000*	5.93×10^2	1.000*
	16	3.11×10^4	0.213	2.23×10^3	0.885	1.51×10^2	1.000*	5.49×10^2	1.000*
	32	3.24×10^4	0.178	2.01×10^3	0.764	7.40×10^1	0.999	4.75×10^2	1.000*
	64	–	–	1.99×10^3	0.631	3.77×10^1	0.997	4.61×10^2	1.000*
	128	–	–	–	–	1.90×10^1	0.998	4.41×10^2	1.000*
	256	–	–	–	–	9.47×10^0	0.998	4.23×10^2	1.000*
Sift	1	1.93×10^4	0.782	3.98×10^3	0.686	6.98×10^2	1.000*	5.52×10^2	1.000
	2	2.03×10^4	0.552	3.80×10^3	0.614	3.30×10^2	1.000*	2.66×10^2	1.000
	4	2.18×10^4	0.394	3.69×10^3	0.637	1.65×10^2	1.000*	1.43×10^2	1.000
	8	2.48×10^4	0.298	3.58×10^3	0.710	7.72×10^1	1.000*	7.94×10^1	1.000
	16	2.68×10^4	0.210	3.50×10^3	0.690	3.98×10^1	1.000*	8.12×10^1	1.000
	32	2.75×10^4	0.193	3.44×10^3	0.639	2.09×10^1	0.999	7.81×10^1	1.000
	64	–	–	3.39×10^3	0.678	8.87×10^0	0.997	7.43×10^1	1.000
	128	–	–	3.36×10^3	0.643	4.78×10^0	0.993	6.80×10^1	1.000
Random	1	1.17×10^4	0.060	4.28×10^3	0.028	7.34×10^2	1.000*	5.54×10^2	1.000
	2	1.01×10^4	0.048	4.04×10^3	0.021	3.58×10^2	1.000*	2.69×10^2	1.000
	4	9.12×10^3	0.031	3.64×10^3	0.014	1.90×10^2	1.000*	1.37×10^2	1.000
	8	8.35×10^3	0.022	3.37×10^3	0.013	8.84×10^1	1.000*	5.69×10^1	1.000
	16	8.25×10^3	0.008	3.17×10^3	0.006	4.36×10^1	1.000*	2.61×10^1	1.000
	32	–	–	3.01×10^3	0.007	1.72×10^1	1.000*	1.35×10^1	1.000

5. Discussion and Future Work.

We have presented CAKES, a set of three algorithms for fast k-NN search that are generic over a variety of distance functions. CAKES's algorithms are exact when the distance function in use is a metric (see definition in 2). Even under cosine distance, which is not a metric, CAKES's algorithms exhibit nearly perfect recall. CAKES's algorithms are designed to be most effective when the data uphold the manifold hypothesis,

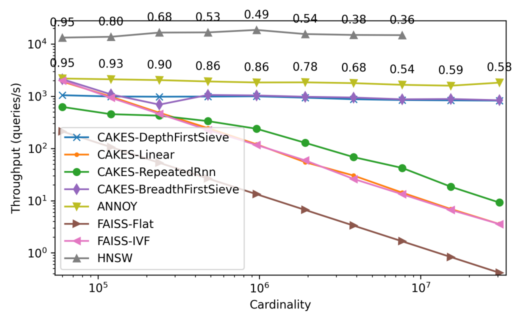

(a) Fashion-Mnist for $k = 10$.

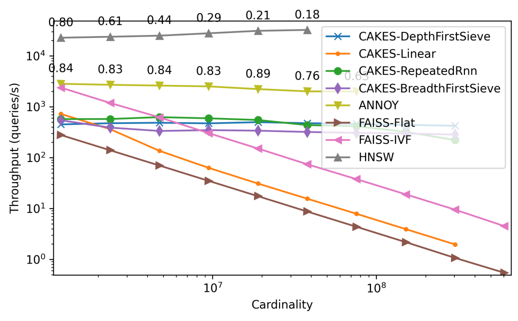

(b) Glove-25 for $k = 10$.

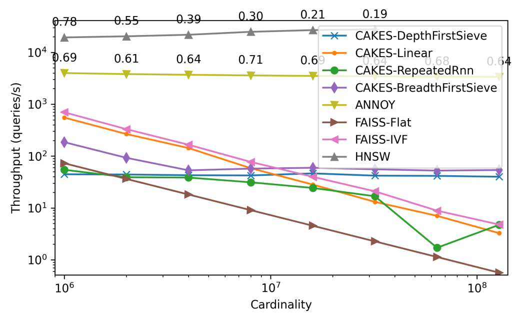

(c) Sift for $k = 10$.

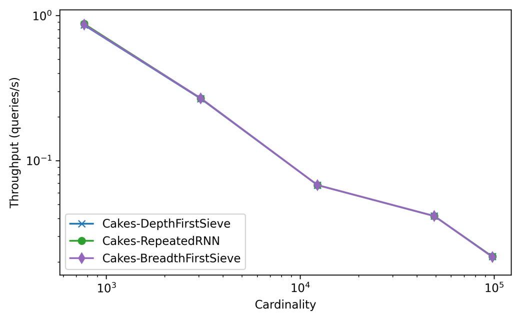

(d) RadioML for $k = 10$ at SnR $= 10$dB.

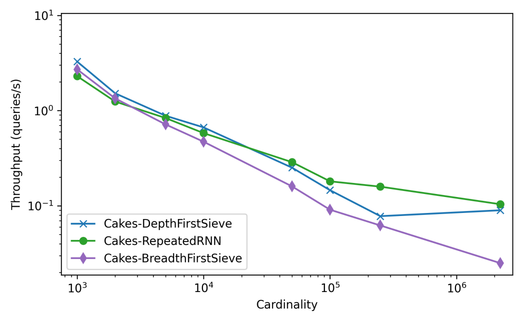

(e) Silva for $k = 10$.

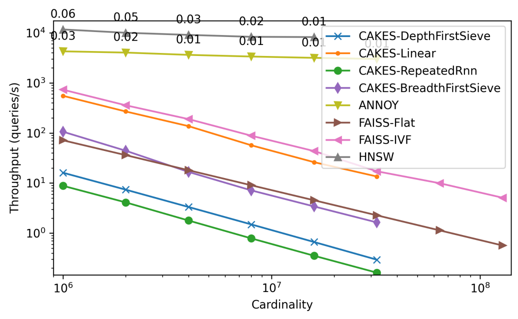

(f) A random dataset for $k = 10$.

Figure 3: Throughput across six datasets, including a randomly-generated dataset. In each plot, the horizontal axis represents increasing cardinality of the dataset, while the vertical axis represents the throughput in queries per second (higher is better). Note that for RadioML, all three algorithms performed nearly identically, so distinct lines are not visible. For some algorithms, we were not able to take measurements for each cardinality because the index-building required more RAM than was available (i.e. more then 512GB).

or in other words, when the data are constrained to a low-dimensional manifold even when embedded in a high-dimensional space. As a consequence, these algorithms do not perform well on data with random distributions, because of the absence of a manifold structure. In Figure 2, we show the extent to which each dataset we tested exhibits a manifold structure, as quantified by the percentiles of LFD. As expected, our results from Figure 3 indicate that CAKES's algorithms scale sub-linearly with cardinality on datasets with low LFD, and scale linearly on datasets with high LFD.

As seen in Figures 2f and 2c, the LFD of the Random dataset is much higher than that of Sift, even though both datasets have the same cardinality and dimensionality. This is unsurprising, given that the Random dataset is uniformly distributed, while Sift is not. On the Random dataset, CAKES's speed decreases linearly as the multiplier increases, while with Sift, Depth-First Sieve and Breadth-First Sieve both exhibit nearly constant throughput. While Repeated ρ-NN does not exhibit near-constant throughput with Sift, throughput decreases much more slowly than it does with the Random dataset. Since these two datasets have the same cardinality and embedding dimension, the aforementioned discrepancies highlight how manifold structure affects algorithm performance. We emphasize that although CAKES's algorithms are slower on the Random dataset, their recalls remain perfect. Figure 3 also shows that HNSW and ANNOY have near-constant throughput as the multiplier increases, but their recall continues to decrease as the multiplier increases. This, coupled with the increasing time and space cost of building the indices for HNSW and ANNOY, makes these algorithms unsuitable for real-world applications in which the datasets are growing exponentially. CAKES's tree is orders of magnitude faster and less memory-intensive to build, and CAKES's algorithms, while slower than HNSW and ANNOY, still show near-constant scaling as well as perfect recall.

When written with the same notation as used in Section 2.4.5, we see that the time complexity of Repeated ρ-NN is $\mathcal{O}(\frac{\mathcal{T}}{\lceil d \rceil} + \mathcal{L})$, where $\mathcal{T}$ is the time complexity of tree-search and $\mathcal{L}$ is the time complexity of leaf-search. Even though Repeated ρ-NN has the lowest time complexity (compare to $\mathcal{O}(\mathcal{T} \log(\mathcal{T} + \mathcal{L}) + \mathcal{L} \log(\mathcal{T} + \mathcal{L}))$ for Breadth-First Sieve and $\mathcal{O}(\mathcal{T} \log \mathcal{T} + \mathcal{L} \log k)$ for Depth-First Sieve) of the three CAKES algorithms, it is not always the fastest algorithm empirically. We believe that some of this discrepancy can be explained by the fact that if Repeated ρ-NN significantly "overshoots" the correct radius for k hits (ρ_k) during tree-search, leaf-search will require looking at more points, rendering the true scaling factor higher than that in Equation 2.4. This overshot can occur when the LFDs of clusters near the query are not concentrated around their expectation. For example, if most clusters near the query have very low LFD except for one anomaly with very high LFD, the harmonic mean LFD μ can still be low, so the factor of radial increase 2.3 may be much larger than necessary for guaranteeing k hits. This suggests that rather than using the reciprocal of the *harmonic* mean LFD in 2.3, we may achieve better results with a mean that is more sensitive to high outliers, such as the geometric mean. We leave it as an avenue for future work to characterize when Repeated ρ-NN significantly "overshoots" ρ_k and to improve upon the factor of radial increase in 2.3 so that this occurs less frequently and with less severity.

As the previous paragraph suggests, the fastest CAKES algorithm varies by dataset. For example, on Glove-25, Repeated ρ-NN exhibits the highest throughput of any CAKES algorithm, despite having the lowest throughput of the three on Sift and Fashion-Mnist. On Silva, Repeated ρ-NN is comparable to the other CAKES algorithms at low multipliers, but becomes the fastest at the higher multipliers. When we view these results in light of the LFD plots in Figure 2, we realize that Repeated ρ-NN appears to be the fastest CAKES algorithm on datasets where a large proportion of the data have a very low LFD, such as Glove-25 and Silva. This trend is unsurprising, given that Repeated ρ-NN relies on a low LFD around the query in order to quickly estimate the correct radius for k hits. These findings suggest that Repeated ρ-NN is the most "sensitive" to the manifold structure of the dataset. Exploring this sensitivity is a potential avenue for future study, as it remains to be seen at what LFD Repeated ρ-NN transitions away from being the fastest CAKES algorithm, and whether this transition is sharp.

While the fastest CAKES algorithm varies by dataset, we note that on all three ANN-benchmark datasets (Fashion-Mnist, Glove-25, and Sift), Depth-First Sieve and Breadth-First Sieve show nearly constant throughput as the cardinality increases. This observation warrants further investigation, but it is especially promising given that both algorithms consistently outperform linear search for high cardinalities. Finally, we emphasize that the variation in performance of our algorithms across different datasets and cardinalities supports our use of an auto-tuning function (as discussed in Section 2.5) to select the best algorithm for a given dataset. Future work is needed to better characterize those datasets for which each algorithm performs best, but our results suggest that a more sophisticated auto-tuning function could be developed to select the fastest algorithm based on the properties of the dataset.

We also stress that CAKES's algorithms are designed to work well for *big* data, and our results support this claim; we observe that while linear search can outperform CAKES on datasets with small cardinality, CAKES always overtakes linear search at a large enough cardinality for each of the ANN-benchmarks' datasets we tested. Moreover, we observe that CAKES's algorithms outperform linear search at a lower cardinality when the dataset has a lower LFD. For example, Sift has much higher LFD than Fashion-Mnist and Glove-25, and we observe that CAKES overtakes linear search at a cardinality of 10^7 for Sift, as opposed to about 10^5 and 10^6 for Fashion-Mnist and Glove-25, respectively. For the Random dataset, which has the highest LFD, CAKES's algorithms *never* outperform linear search. These observations support our claim that CAKES performs well on datasets that arise from constrained generating phenomena, even as the cardinalities of these datasets grow exponentially.

The questions raised by this study suggest several additional avenues for future work. A comparison across more datasets is in order, as is further analysis with other distance functions that existing methods, such as FAISS, HNSW and ANNOY, do not support, such as Wasserstein distance [36] for probability distributions (particularly for high dimensional distributions), and Tanimoto distance [4] for comparing molecular structures by their maximal common subgraphs. Incorporating these or other distance functions in CAKES requires only that a Rust implementation of the distance function be provided.

We also plan to investigate hierarchical data compression by representing differences at each level of the binary tree, particularly for string or genomic data, where all differences are discrete. Such an encoding would allow us to store the data in a compressed format, and to perform search on the compressed data without decompressing it. This would allow us to perform fast search on datasets that are too large to fit in memory. An exploration of compression and compressed search is another avenue for future work.

We also would like to explore the use of CAKES in a streaming environment. This would require the ability to perform "online" updates to the tree as points are added to or deleted from the dataset. Such online updates would take advantage of the fast search algorithms provided by CAKES. CAKES can also be used to extend anomaly detection in CHAODA [17]. We could add to CHAODA's ensemble of graph-based anomaly detection methods by using the distribution of distances among the k nearest neighbors of cluster centers.

CLAM and CAKES are implemented in Rust and the source code is available under an MIT license at https://github.com/URI-ABD/clam.

REFERENCES

[1] *Faiss-ivf*. https://github.com/facebookresearch/faiss/wiki/Faiss-indexes, 2016.

[2] M. Aumüller, E. Bernhardsson, and A. Faithfull, *Ann-benchmarks: A benchmarking tool for approximate nearest neighbor algorithms*, Inf. Syst., 87 (2018).

[3] M. Aumüller, E. Bernhardsson, and A. Faithfull, *Ann-benchmarks: A benchmarking tool for approximate nearest neighbor algorithms*, Information Systems, 87 (2020), p. 101374.

[4] D. Bajusz, A. Rácz, and K. Héberger, *Why is tanimoto index an appropriate choice for fingerprint-based similarity calculations?*, Journal of cheminformatics, 7 (2015), pp. 1–13.

[5] E. Bernhardsson, *Annoy*. https://github.com/spotify/annoy, 2015.

[6] M. Boguna, D. Krioukov, and K. C. Claffy, *Navigability of complex networks*, Nature Physics, 5 (2009), pp. 74–80.

[7] T. B. Brown, B. Mann, N. Ryder, M. Subbiah, J. Kaplan, P. Dhariwal, A. Neelakantan, P. Shyam, G. Sastry, A. Askell, S. Agarwal, A. Herbert-Voss, G. Krueger, T. Henighan, R. Child, A. Ramesh, D. M. Ziegler, J. Wu, C. Winter, C. Hesse, M. Chen, E. Sigler, M. Litwin, S. Gray, B. Chess, J. Clark, C. Berner, S. McCandlish, A. Radford, I. Sutskever, and D. Amodei, *Language Models are Few-Shot Learners*, arXiv e-prints, (2020), arXiv:2005.14165, p. arXiv:2005.14165, https://doi.org/10.48550/arXiv.2005.14165, https://arxiv.org/abs/2005.14165.

[8] I. Budowski-Tal, Y. Nov, and R. Kolodny, *Fragbag, an accurate representation of protein structure, retrieves structural neighbors from the entire pdb quickly and accurately*, Proceedings of the National Academy of Sciences, 107 (2010), pp. 3481–3486.

[9] T. M. Cover, P. Hart, et al., *Nearest neighbor pattern classification*, IEEE transactions on information theory, 13 (1967), pp. 21–27.

[10] A. Dosovitskiy, L. Beyer, A. Kolesnikov, D. Weissenborn, X. Zhai, T. Unterthiner, M. Dehghani, M. Minderer, G. Heigold, S. Gelly, et al., *An image is worth 16x16 words: Transformers for image recognition at scale*, arXiv preprint arXiv:2010.11929, (2020).

[11] C. Fefferman, S. Mitter, and H. Narayanan, *Testing the manifold hypothesis*, Journal of the American Mathematical Society, 29 (2016), pp. 983–1049.

[12] E. Fix and J. L. Hodges Jr, *Discriminatory analysis-nonparametric discrimination: Small sample performance*, tech. report, California Univ Berkeley, 1952.

[13] J. Gao and C. Long, *High-dimensional approximate nearest neighbor search: with reliable and efficient distance comparison operations*, Proceedings of the ACM on Management of Data, 1 (2023), pp. 1–27.

[14] O. Gold and M. Sharir, *Dynamic time warping and geometric edit distance: Breaking the quadratic barrier*, ACM Transactions on Algorithms (TALG), 14 (2018), pp. 1–17.

[15] C. A. Hoare, *Algorithm 65: find*, Communications of the ACM, 4 (1961), pp. 321–322.

[16] L.-Y. Hu, M.-W. Huang, S.-W. Ke, and C.-F. Tsai, *The distance function effect on k-nearest neighbor classification for medical datasets*, SpringerPlus, 5 (2016), pp. 1–9.

[17] N. Ishaq, T. J. Howard, and N. M. Daniels, *Clustered hierarchical anomaly and outlier detection algorithms*, in 2021 IEEE International Conference on Big Data (Big Data), IEEE, 2021, pp. 5163–5174.

[18] N. Ishaq, G. Student, and N. M. Daniels, *Clustered hierarchical entropy-scaling search of astronomical and biological data*, in 2019 IEEE International Conference on Big Data (Big Data), IEEE, 2019, pp. 780–789.

[19] J. Johnson, M. Douze, and H. Jégou, *Billion-scale similarity search with GPUs*, IEEE Transactions on Big Data, 7 (2019), pp. 535–547.

[20] S. D. Kahn, *On the future of genomic data*, Science, 331 (2011), pp. 728–729.
[21] A. Kent, R. Sacks-Davis, and K. Ramamohanarao, *A signature file scheme based on multiple organizations for indexing very large text databases*, Journal of the american society for information science, 41 (1990), pp. 508–534.
[22] J. M. Kleinberg, *Navigation in a small world*, Nature, 406 (2000), pp. 845–845.
[23] V. I. Levenshtein et al., *Binary codes capable of correcting deletions, insertions, and reversals*, in Soviet physics doklady, vol. 10, Soviet Union, 1966, pp. 707–710.
[24] Y. Malkov and D. A. Yashunin, *Efficient and robust approximate nearest neighbor search using hierarchical navigable small world graphs*, IEEE Transactions on Pattern Analysis and Machine Intelligence, 42 (2016), pp. 824–836, https://api.semanticscholar.org/CorpusID:8915893.
[25] Y. A. Malkov and D. A. Yashunin, *Efficient and robust approximate nearest neighbor search using hierarchical navigable small world graphs*, CoRR, abs/1603.09320 (2016), http://arxiv.org/abs/1603.09320, https://arxiv.org/abs/1603.09320.
[26] M. Müller, *Dynamic time warping*, Information retrieval for music and motion, (2007), pp. 69–84.
[27] OpenAI, *Gpt-4 technical report*, ArXiv, abs/2303.08774 (2023).
[28] T. J. O'Shea, T. Roy, and T. C. Clancy, *Over-the-air deep learning based radio signal classification*, IEEE Journal of Selected Topics in Signal Processing, 12 (2018), pp. 168–179, https://doi.org/10.1109/JSTSP.2018.2797022.
[29] C. Quast, E. Pruesse, P. Yilmaz, J. Gerken, T. Schweer, P. Yarza, J. Peplies, and F. O. Glöckner, *The SILVA ribosomal RNA gene database project: improved data processing and web-based tools*, Nucleic Acids Research, 41 (2012), pp. D590–D596, https://doi.org/10.1093/nar/gks1219, https://arxiv.org/abs/https://academic.oup.com/nar/article-pdf/41/D1/D590/3690367/gks1219.pdf.
[30] A. Radford, J. W. Kim, C. Hallacy, A. Ramesh, G. Goh, S. Agarwal, G. Sastry, A. Askell, P. Mishkin, J. Clark, et al., *Learning transferable visual models from natural language supervision*, in International conference on machine learning, PMLR, 2021, pp. 8748–8763.
[31] R. Sacks-Davis, A. Kent, and K. Ramamohanarao, *Multikey access methods based on superimposed coding techniques*, ACM Transactions on Database Systems (TODS), 12 (1987), pp. 655–696.
[32] S. Suyanto, P. E. Yunanto, T. Wahyuningrum, and S. Khomsah, *A multi-voter multi-commission nearest neighbor classifier*, Journal of King Saud University - Computer and Information Sciences, 34 (2022), pp. 6292–6302, https://doi.org/https://doi.org/10.1016/j.jksuci.2022.01.018.
[33] H. Touvron, L. Martin, K. R. Stone, P. Albert, A. Almahairi, Y. Babaei, N. Bashlykov, S. Batra, P. Bhargava, S. Bhosale, D. M. Bikel, L. Blecher, C. C. Ferrer, M. Chen, G. Cucurull, D. Esiobu, J. Fernandes, J. Fu, W. Fu, B. Fuller, C. Gao, V. Goswami, N. Goyal, A. S. Hartshorn, S. Hosseini, R. Hou, H. Inan, M. Kardas, V. Kerkez, M. Khabsa, I. M. Kloumann, A. V. Korenev, P. S. Koura, M.-A. Lachaux, T. Lavril, J. Lee, D. Liskovich, Y. Lu, Y. Mao, X. Martinet, T. Mihaylov, P. Mishra, I. Molybog, Y. Nie, A. Poulton, J. Reizenstein, R. Rungta, K. Saladi, A. Schelten, R. Silva, E. M. Smith, R. Subramanian, X. Tan, B. Tang, R. Taylor, A. Williams, J. X. Kuan, P. Xu, Z. Yan, I. Zarov, Y. Zhang, A. Fan, M. Kambadur, S. Narang, A. Rodriguez, R. Stojnic, S. Edunov, and T. Scialom, *Llama 2: Open foundation and fine-tuned chat models*, ArXiv, abs/2307.09288 (2023), https://api.semanticscholar.org/CorpusID:259950998.
[34] N. Ukey, Z. Yang, B. Li, G. Zhang, Y. Hu, and W. Zhang, *Survey on exact knn queries over high-dimensional data space*, Sensors, 23 (2023), p. 629.
[35] E. Ukkonen, *Algorithms for approximate string matching*, Information and control, 64 (1985), pp. 100–118.
[36] S. Vallender, *Calculation of the wasserstein distance between probability distributions on the line*, Theory of Probability & Its Applications, 18 (1974), pp. 784–786.
[37] Y. W. Yu, N. Daniels, D. C. Danko, and B. Berger, *Entropy-scaling search of massive biological data*, Cell Systems, 1 (2015), pp. 130–140.
[38] J. Zhang, T. Wang, W. W. Ng, and W. Pedrycz, *Ensembling perturbation-based oversamplers for imbalanced datasets*, Neurocomput., 479 (2022), p. 1–11, https://doi.org/10.1016/j.neucom.2022.01.049, https://doi.org/10.1016/j.neucom.2022.01.049.
[39] P. Zhang, *Privacy preserving similarity search for online advertising*, (2020).